

1
> REPLACE THIS LINE WITH YOUR PAPER IDENTIFICATION NUMBER (DOUBLE-CLICK HERE TO EDIT) <

Miniaturization of TEM Horn Using Spherical Modes Engineering

Mohamed A. Elmansouri, *Member, IEEE*, Dejan S. Filipovic, *Senior Member, IEEE*

Abstract—The spherical mode expansion (SME) is exploited to miniaturize a transverse electromagnetic (TEM) horn antenna and achieve good frequency and time domain performances. To adjust the radiated powers of fundamental TE and TM modes, the combined loop and TEM horn antenna is engineered. The constructive combination of the two modes below the horn's turn-on frequency miniaturizes the antenna and improves its gain. The magnitude and phase tuning of the desired modes is achieved by modifying the loop's geometry. The spherical modal spectrum at higher frequencies is also studied and antenna's geometry is further modified to maintain constructive interference between the higher order spherical modes. A prototype with electrical size of $0.188\lambda \times 0.145\lambda \times 0.087\lambda$ (length \times width \times height) at the turn-on frequency is fabricated over a ground plane. Over 3 times lower turn-on frequency is obtained compared to a conventional TEM horn with up to 9dB improvement in the realized gain at the low end and better radiation characteristics over more than 5:1 bandwidth (from 0.87GHz to 4.5GHz). Unidirectional operation with front to back ratio >9dB and excellent time-domain performance with fidelity factor >95% over wide field of view are also demonstrated.

Index Terms— Antenna miniaturization, fidelity factor, spherical modes expansion, TEM horn, wideband operation.

I. INTRODUCTION

THE extremely-wideband, nearly dispersion-less characteristics, and simple structure of the transverse electromagnetic (TEM) horn make this antenna a viable candidate for variety of ultra-wideband (UWB) communication, radar, and pulse radiation applications [1]-[2]. Design of TEM horns is addressed in different places in literature and good performance over more than a decade bandwidth is demonstrated [3]-[6]. However, the persistent issue with these conventional designs is the horn's size. The length and the opening at the TEM horn aperture need to be $\sim\lambda/2$ at the desired lowest frequency of operation in order for the antenna to operate efficiently. This is quite large when intended use is at VHF/UHF frequencies. The typical approach to reduce TEM horn size and improve its low-end performance relies on eliminating the reflected currents from its aperture. This is achieved by optimizing aperture shape to carefully match its impedance to free space [5]-[8] or by dissipating the reflected currents in resistors or ferrite chokes

[9]-[10]. However, the aperture shaping leads to small miniaturization factor; whereas the loss-loading approach significantly degrades radiation efficiency at low frequencies. Dielectric loading is also applied to reduce the phase velocity of the travelling wave and establish radiation below the designated turn-on frequency [11]. However, increased mismatch between antenna opening and free space deteriorates gain and radiation patterns. Multi-layer graded dielectric profile [10]-[11] can help at the expense of increased design complexity and weight. An interesting strategy, originally proposed in [12], to simultaneously reduce the turn-on frequency and improve gain is the combined antenna approach. There, the TEM horn is combined with metallic loop(s) and associated electric (i.e. TEM horn) and magnetic (i.e. loop) moments at low frequencies are balanced to achieve enhanced radiation characteristics and better impedance match at the low frequency end. However, fulfilling the moments balancing condition at low frequencies while maintaining good performance over the operating band is challenging [13]-[18] and requires a systematic design method.

In this paper, the spherical modes expansion (SME) [19] is used to enable the design and miniaturization of combined TEM horn and loop antenna. SME assists in understanding the antenna behavior at both low and high frequencies. At low end, SME can help in better understanding and then miniaturizing the antennas by proper engineering of modal spectrum; whereas at higher frequencies, it can aid in tailoring the modal spectrum to achieve high gain and front to back ratio (F/B). Full-wave simulation studies based on method of moments (MOM) as implemented in FEKO [20] are conducted to find the connection between the antenna geometry modifications and expanded spherical modes. Based on these studies, to achieve the desired combination between the fundamental modes, a simple current perturbation approach is implemented by adding crescent slots to the loop. The rectangular loop geometry is also modified to realize the coherent superposition between the higher order modes over wide bandwidth. The fabricated prototype, shown in Fig. 1, has 3 times lower turn-on frequency and up to 9dB increased realized gain at the low end compared to a conventional TEM horn. In addition, F/B, gain, patterns, and miniaturization factor are improved compared to other proposed combined antennas with the same physical dimensions [13]-[18].

This paper is organized as follows: Section II outlines the theoretical framework that led to the designed antenna. Section III discusses the combined antenna design and the proposed geometrical modifications needed to engineer the desired spherical modes. The realized antenna and its

This work was supported by the Office of Naval Research (ONR) award # N00014-13-1-10537.

The authors are with the Department of Electrical, Computer, and Energy Engineering, University of Colorado Boulder, CO 80309-0425 USA (e-mail: { mohamed.elmansouri,dejan }@colorado.edu).

2
> REPLACE THIS LINE WITH YOUR PAPER IDENTIFICATION NUMBER (DOUBLE-CLICK HERE TO EDIT) <

measured frequency- and time-domain performances are presented in Section IV.

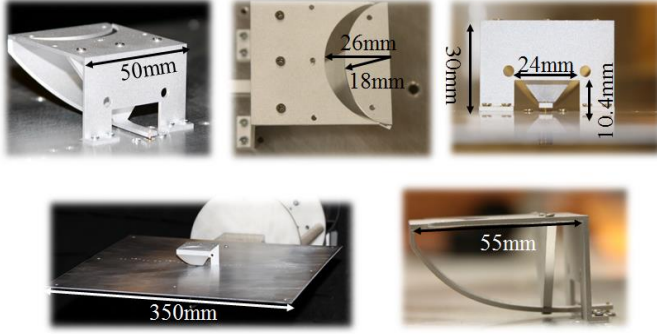


Fig. 1. Photographs of the fabricated combined antenna over a ground plane.

II. SPHERICAL MODES ENGINEERING

The radiated electric fields from an antenna can be expanded at any distance into a set of orthogonal transverse (to radial distance r) magnetic (TM) and electric (TE) spherical modes as [19],[21]

$$\vec{E}(\vec{r}) = \sum_{m=-n}^n \sum_{n=1}^{\infty} b_{mn}^{(TE)} \vec{M}_{mn}(\vec{r}) + b_{mn}^{(TM)} \vec{N}_{mn}(\vec{r}) \quad (1)$$

where $b_{mn}^{(TE)}$ and $b_{mn}^{(TM)}$ are the TE and TM modal coefficients, respectively; m and n are the mode indices ($|m| \leq n$). $\vec{M}_{mn}(\vec{r})$ and $\vec{N}_{mn}(\vec{r})$ are the normalized vector spherical harmonics which can be written for the far-field case as,

$$\vec{M}_{mn}(\vec{r}) = j^{n+1} \frac{e^{-jkr}}{kr} \vec{\mathcal{K}}_{mn}(\theta, \varphi) \quad (2.a)$$

$$\vec{N}_{mn}(\vec{r}) = j^n \frac{e^{-jkr}}{kr} \hat{r} \times \vec{\mathcal{K}}_{mn}(\theta, \varphi) \quad (2.b)$$

Where

$$\vec{\mathcal{K}}_{mn}(\theta, \varphi) = \left(-\frac{m}{|m|}\right)^m \sqrt{\frac{(2n+1)(n-|m|)!}{4\pi n(n+1)(n+|m|)}} e^{jm\varphi} \cdot \left[\frac{jm}{\sin\theta} P_n^{|m|}(\cos\theta) \hat{\theta} - \frac{\partial}{\partial\theta} (P_n^{|m|}(\cos\theta)) \hat{\varphi} \right] \quad (3)$$

$P_n^m(x)$ is the associated Legendre function and $h_n^{(2)}(kr)$ is the spherical Hankel function of the second kind. The antenna's total radiated power P_{rad} and directivity D can be also expressed through the modal coefficients as [19],

$$\begin{aligned} P_{rad} &= \frac{1}{2} \int_0^{2\pi} \int_0^{\pi} \text{Re}[(\vec{E} \times \vec{H}^*) \cdot \hat{r}] r^2 \sin\theta \, d\theta \, d\varphi \\ &= \frac{1}{2} \sum_{mn} |b_{mn}^{(TE)}|^2 + |b_{mn}^{(TM)}|^2 \end{aligned} \quad (4)$$

$$\begin{aligned} D(\theta, \varphi) &= \frac{|\sum_{mn} b_{mn}^{(TE)} \vec{\mathcal{K}}_{mn}(\theta, \varphi) + \sum_{mn} b_{mn}^{(TM)} (\hat{r} \times \vec{\mathcal{K}}_{mn}(\theta, \varphi))|^2}{\sum_{mn} |b_{mn}^{(TE)}|^2 + |b_{mn}^{(TM)}|^2} \end{aligned} \quad (5)$$

Electrically small antennas radiate only the fundamental TE or TM mode ($n = 1$). As the antenna electrical size increases, higher-order spherical modes radiate and the combination thereof determines the antenna characteristics as seen from above equations. Thus, arbitrary radiation patterns can be synthesized by computing the required magnitude and phase of $b_{mn}^{(TE)}/b_{mn}^{(TM)}$ to achieve the desired combination. The chief challenge is to find one-to-one correspondence between the radiated spherical modes and the antenna's physical structure particularly if many spherical modes are radiated (i.e. electrically-large antennas). The analysis is simplified for modest electrical size antenna since its radiation can be represented by few spherical modes. Only modes with $n < ka$ (where a is the radius of the minimum sphere enclosing the antenna) are of importance to represent the antenna radiation in this case [19].

P×M antenna [22]-[23] is an example of combining constructively the appropriate spherical modes to improve the directivity. Specifically, the fundamental TM_{m1} (electric dipole mode) and TE_{m1} (magnetic dipole mode) are combined to generate the hypothetical Huygens source patterns with improved radiation in the forward direction and no backward radiation. Fig. 2 shows a simple realization of this concept by collocating an electrically-small dipole and center-fed loop (i.e. magnetic dipole) [22]. The corresponding spherical mode spectrum of these sources is shown in Fig. 2. The demonstrated relative mode power, which is defined as the ratio between the mode's power and the total radiated power, shows that the elementary y-oriented electric dipole and loop (in yz-plane) radiate only the fundamental TM_{11}/TM_{-11} and TE_{11}/TE_{-11} modes, respectively as expected from their size and orientation [24].

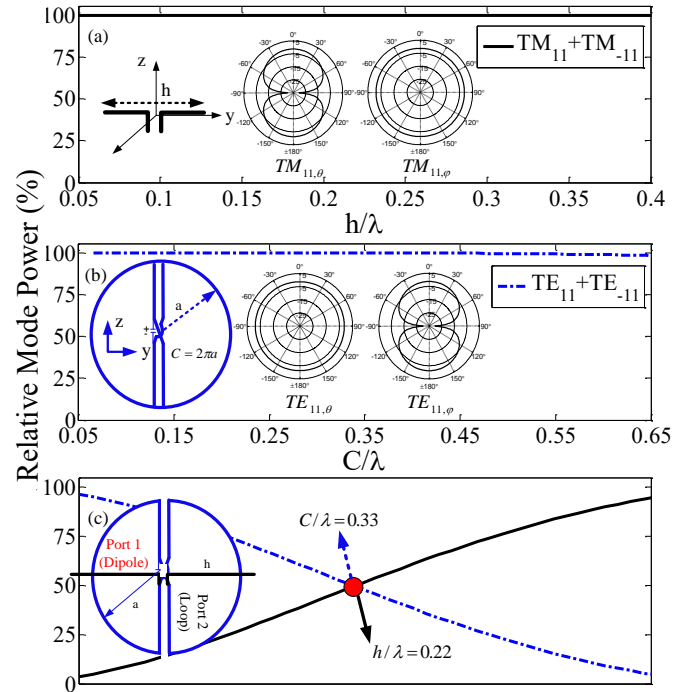


Fig. 2. Spherical mode spectrum of (a) a y-oriented dipole, (b) center-fed loop, and (c) collocated dipole and loop (spacing between the elements is $\lambda_b/20$; where λ_b is the wavelength at the balancing frequency). Fundamental TM_{11}/TE_{11} modes patterns are also shown in the inset.

If a dipole (oriented along y-axis) and center-fed loop (oriented in yz-plane) are collocated and excited using two sources as shown in Fig.2 (c), the total radiated field will be simply the superposition of the loop and the dipole radiation. Thus, the spherical mode spectrum will contain both TE and TM modes. At certain frequency defined by the dipole and loop dimensions and the separation between them (see Fig. 2(c)), the orthogonal dipole (electric) and loop (magnetic) moments are balanced and equal radiation from the TM and TE modes is observed. The maximum achievable directivity (at the broadside direction in this specific case) [25],

$$D_{max} = N^2 + 2N \quad (6)$$

N is the maximum number of n . According to (6), for $N=1$, $D_{max} = 3$ (4.77dB). However, this is only obtained if the modal coefficients are weighted and phased as [19],

$$b_{1n}^{(TM)} = b_{-1n}^{(TM)} = -b_{1n}^{(TE)} = b_{-1n}^{(TE)} \quad (7)$$

When the dipole/loop are excited in phase, the radiated TM_{11}/TE_{11} modes of the dipole/loop are 90° out of phase resulting in an omnidirectional pattern at the balancing frequency as shown in Fig. 3 (a). To satisfy the criterion in (7), the phase of the radiated spherical modes is tuned by exciting the antennas with 90° phase difference. The obtained radiation pattern, shown in Fig. 3(b), exhibits the desired cardioid shape with maximum directivity of 3(4.77dBi) and negligible back radiation. Also, the radiation Q of this configuration is approximately half that of an isolated dipole or loop which should in principle facilitate wider impedance match [23],[26].

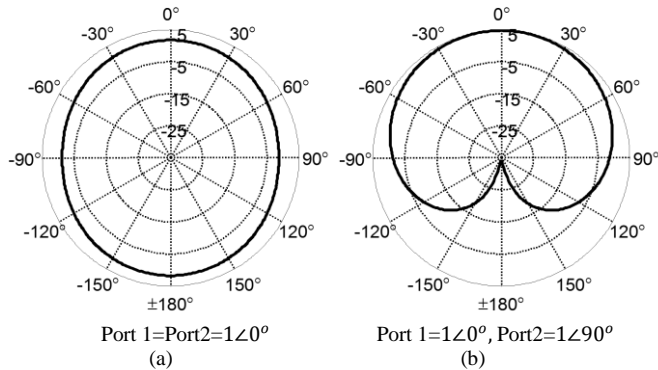


Fig.3. Radiation patterns of the collocated dipole and loop at the modes-balancing frequency (along xz-plane) when they are excited: (a) in phase and (b) with 90° phase difference.

As mentioned, balancing the electric and magnetic dipole moments approach (i.e. balancing the radiation of TM_{m1} and TE_{m1} spherical modes) is considered to improve the performance of the TEM horn at low frequencies. In [12]-[13], a TEM horn (which resembles a small V-dipole at low frequencies ($ka < 1$)) is combined with a rectangular metallic loop. Resistors are distributed along the loop to tune the moments and achieve the balancing condition. Although the impedance match is improved, the radiation efficiency significantly degraded at the low end due to the power loss in resistors. Lossless combined TEM horn/loop configurations are also proposed [14]-[16]; however, the expected

miniaturization effect and gain improvement are not demonstrated. The combined antenna which integrates asymmetric TEM horn with multiple loops is also designed to reduce the reactive energy around the antenna and improve the impedance match at low frequencies [17]-[18]. The balancing condition is achieved by optimizing the size and the location of integrated loops. The modes balancing technique and the improved radiation performance are not explicitly discussed. The aforementioned studies focus on combining the modes at the low end; yet, the higher-order modes of the combined structure may superimpose destructively leading to a degraded radiation performance over certain bandwidth. A systematic design approach is required to achieve the desired radiation characteristics of the combined-mode antenna over the desired bandwidth of operation. In the following sections, the feasibility of utilizing the spherical mode analysis to engineer the desired far-field characteristics of combined antenna will be demonstrated. The considered approach attempts to correlate the implemented structural changes to the radiated modes enabling a simple and insightful design methodology.

III. ENHANCED COMBINED ANTENNA DESIGN

The baseline design, shown in Fig. 4(a), is an exponentially-tapered TEM horn designed following [4], [5] to match 50Ω at the parallel plate feed to the free-space impedance at the antenna's aperture. To achieve a (VSWR=2) turn-on frequency at 3GHz, the physical dimensions of the antenna are $L_h = S_a = W_a = 5\text{cm}$ ($\lambda_{3\text{GHz}}/2$), $W_f = 0.98\text{cm}$, $S_f = 0.2\text{cm}$, and $L_f = 1.5\text{cm}$. Fig. 4(b) shows the proposed combined TEM horn geometry which will be discussed in details in this Section.

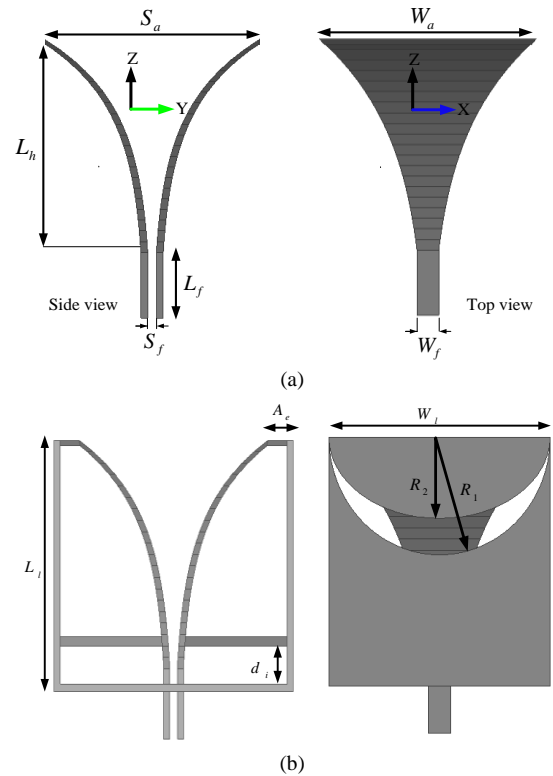


Fig.4. (a) Studied TEM horn and (b) proposed combined antenna with marked geometrical parameters.

The spherical mode spectrum of the baseline design is shown in Fig. 5(a). Modal coefficients are extracted by Hermitian inner product between the simulated radiated far-fields (obtained from FEKO) and the vector spherical harmonics in (2) [20]. For clarity, only modes with $m = \pm 1$, and $n = 1, 2$, and 3 are depicted. Note >85% of the total radiated power is concentrated in these modes over the considered frequency range. At 3GHz ($ka \approx 3$), ~95% of the power is radiated in these modes which agrees with the discussion in the previous Section and implies that the radiation characteristics of the antenna can be represented adequately with these modes and the combination thereof over the desired bandwidth of operation. As expected, when $ka < 1$ (i.e. ~below 1GHz), the conventional TEM horn radiates predominately the y-oriented electric dipole modes ($TM_{\pm 11}$). Notice that the power radiates equally in $m = 1$ and -1 modes. As the electrical size increases (i.e. frequency increases), higher-order TM modes start to radiate as shown in Fig. 5(a).

To excite the fundamental TE mode, the TEM horn is combined with a rectangular loop routed behind the antenna as shown in the inset of Fig. 5(b). A small vertical extension ($A_e = 5\text{mm}$) is added at the TEM horn opening as shown in Fig. 4(b). This extension allows the traveling wave currents reaching the horn opening to transit smoothly to the loop part enabling better impedance match (i.e. less reflection from the aperture) [27]. The loop ($L_l = 5.5\text{cm}$) radiates predominantly the fundamental $TE_{\pm 11}$ modes below 0.5GHz. As the frequency increases, the rectangular loop also contributes to the radiation of the electric dipole modes ($TM_{\pm 11}$) and the higher order $TM_{\pm 12}$ and $TE_{\pm 12}$ modes due to the currents distribution and the loop's orientation [28]. Balancing the modes of this combined antenna at or below 0.5 GHz ($ka \leq 0.5$) is impractical since the antenna cannot be matched to finite source impedance without the aid of an external matching network. Moreover, the phase difference between the TM_{11}/TE_{11} modal coefficients, shown in Fig. 6(a), does not satisfy the criterion in (7). For this electrical size, it is quite challenging to tune the phase of modal coefficients using a single source. According to [29, Fig. 6], the smallest electrical size of UWB antenna to achieve good impedance match (i.e. $VSWR \leq 2$) when the fundamental TM and TE modes are simultaneously excited is $ka = 0.75$. Therefore, to make this approach more practical and obtain the maximum size reduction while maintaining low VSWR, the modes need to be balanced when the antenna electrical size (ka) is 0.75 or larger. The phase difference between the modes TM_{11}/TE_{11} needs to be also tuned to approach 180° in order to achieve the desired gain improvement at the low end. Another issue with the conventional combined loop/TEM horn is the combination between the fundamental and the higher-order modes. Specifically, $TM_{\pm 11}$ and $TM_{\pm 12}$ around 2GHz ($ka \approx 2$) add destructively in the forward direction (along $+z$ -axis) due to the phase difference between the modal coefficients shown in Fig. 6(b). To achieve the desired constructive combination, the coefficients ideally have to be equal and phased as,

$$b_{11}^{(TM)} = b_{-11}^{(TM)} = -jb_{12}^{(TM)} = -jb_{-12}^{(TM)} \quad (8)$$

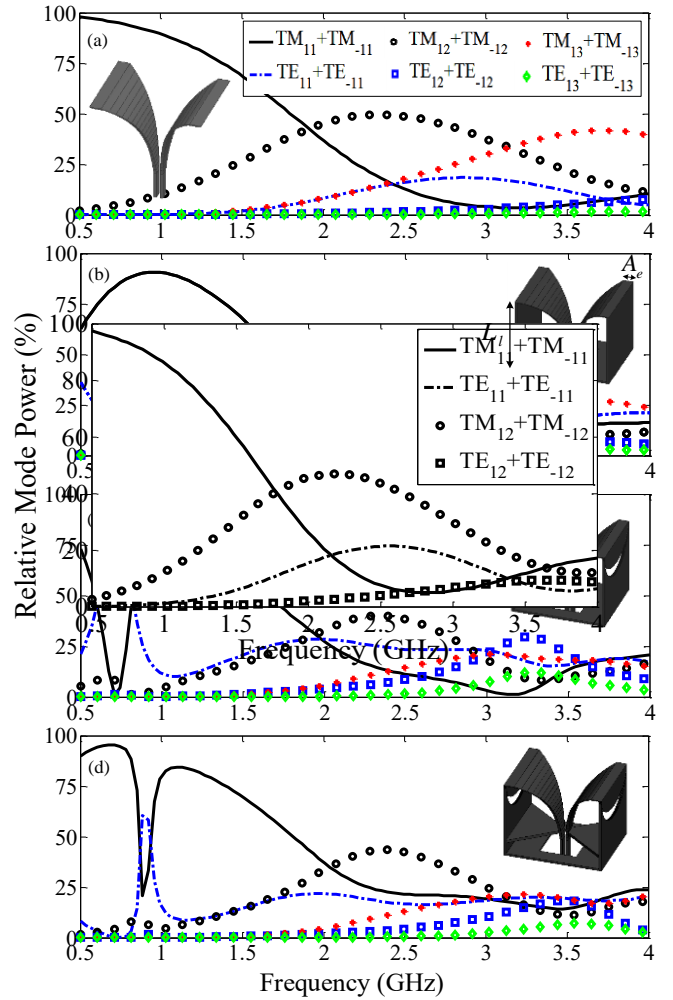


Fig.5. Spherical mode spectrum of (a) conventional TEM horn, (b) combined TEM horn and loop, (c) combined antenna with the perturbation crescent slots, and (d) with the inserted plates (i.e. final configuration). Notice that the total radiated power is 1W.

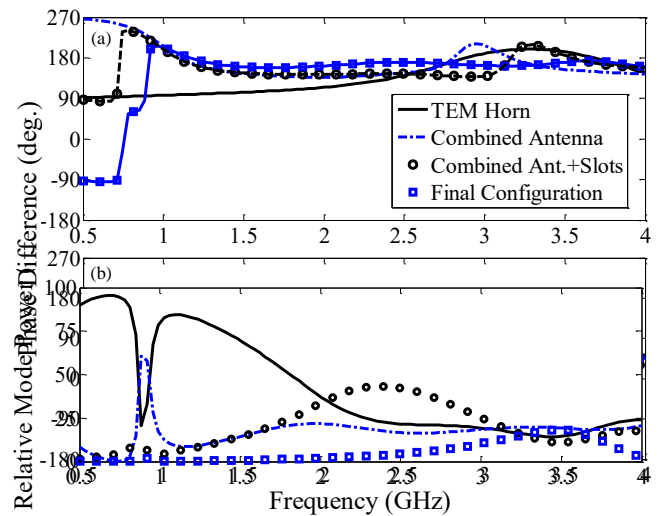


Fig.6. Phase difference between the modal coefficients for different configurations: (a) $\angle b_{11}^{(TM)} - \angle b_{11}^{(TE)}$ and (b) $\angle b_{11}^{(TM)} - \angle b_{12}^{(TM)}$.

Fig. 7 shows the theoretical directivity patterns of $TM_{\pm 11}/TM_{\pm 12}$ modes combination obtained from (5) when $|b_{\pm 11}^{(TM)}| = |b_{\pm 12}^{(TM)}|$ and the phase difference ($\angle b_{11}^{(TM)} -$

$\angle b_{12}^{(TM)}$) between the coefficients is $\pm 90^\circ$. As seen, phase difference of $+90^\circ$ is required to achieve the desired radiation characteristics. If the phase difference is negative and approaching -90° , the peak radiation will be in the backward direction and gain dip will show up in the broadside direction which is the case of the combined antenna according to the phase difference in Fig. 6(b). Changing the loop length tunes the phase difference; however, the conducted numerical studies show that increasing the length leads to more destructive interference whereas decreasing it limits the advantages of using the loop [27]. The VSWR, broadside gain, and F/B of the combined antenna along with those of the conventional TEM horn and the other proposed configurations are shown in Figs. 8 (a),(b), and (c); respectively. Impedance match of the combined antenna is improved compared to the conventional TEM horn, and (VSWR=2) turn-on frequency is reduced from 3GHz to 1.1GHz. Two mechanisms contribute in the impedance match improvement at the low end; significant decrease in reflections from the horn's aperture and reduction of capacitive reactive energy around the antenna due to the inductive loop [18]. Although the match is improved, no noticeable improvement in the gain is observed at the low end as expected from the spherical mode spectrum. The drop in the gain and F/B around 2GHz is due to the discussed destructive interference of $TM_{\pm 11}/TM_{\pm 12}$ modes.

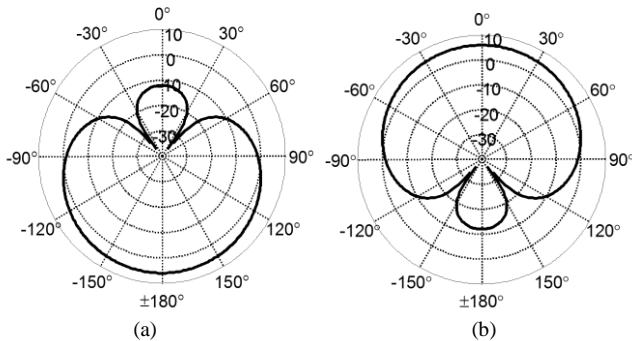


Fig.7. Directivity patterns of the TM_{11}/ TM_{-11} and TM_{12}/ TM_{-12} combination along xz -plane (a) phase difference ($\angle b_{11}^{(TM)} - \angle b_{12}^{(TM)}$) is -90° and (b) $+90^\circ$.

The presented spherical modes analysis shows the main issues with the combined antenna design and points to the specific features that may be improved. To address the first issue i.e. the appropriate excitation of the fundamental TE mode, a simple approach based on adding current perturbation slots to the loop is researched. Slot configurations, particularly in large ground plane, can radiate the fundamental TE mode if they are appropriately excited. Even though these conditions are not fully fulfilled herein, the implemented slots can still perturb the surface currents on the loop and enable the radiation of fundamental TE mode. The location, shape, and size of the slot determine the characteristics of the radiated mode. The conducted numerical studies show that adding slots to the bottom and the top plates of the loop at the interface with the TEM horn, as shown in the inset of Fig. 5(c), tune the excitation of the fundamental TE mode. Different slot shapes are considered including crescent, elliptical, and triangular. A mode-balancing frequency approaching the designated frequency ($f = 0.75\text{GHz}$, $ka \approx 0.75$) is obtained with the crescent slots. As shown in Fig. 5(c), TM/TE balancing

condition at 0.84GHz ($ka \approx 0.84$) is achieved with crescent slots with major (R_1) and minor (R_2) radii of 2.6cm and 1.8cm ; respectively. The fundamental TM and TE modes add coherently in forward direction since the phase difference between the modal coefficients is approaching the desired value of 180° as shown in Fig. 6(a). Varying R_1 or R_2 helps tune the magnitude and phase of the radiated fundamental modes as will be discussed later in this Section. The addition of the slots also helps mitigating the issue of the undesired combination between $TM_{\pm 11}/TM_{\pm 12}$ modes by tuning the phase difference between the modal coefficients. As shown in Fig. 6(b), the phase difference is approaching a positive value leading to more radiation in forward direction.

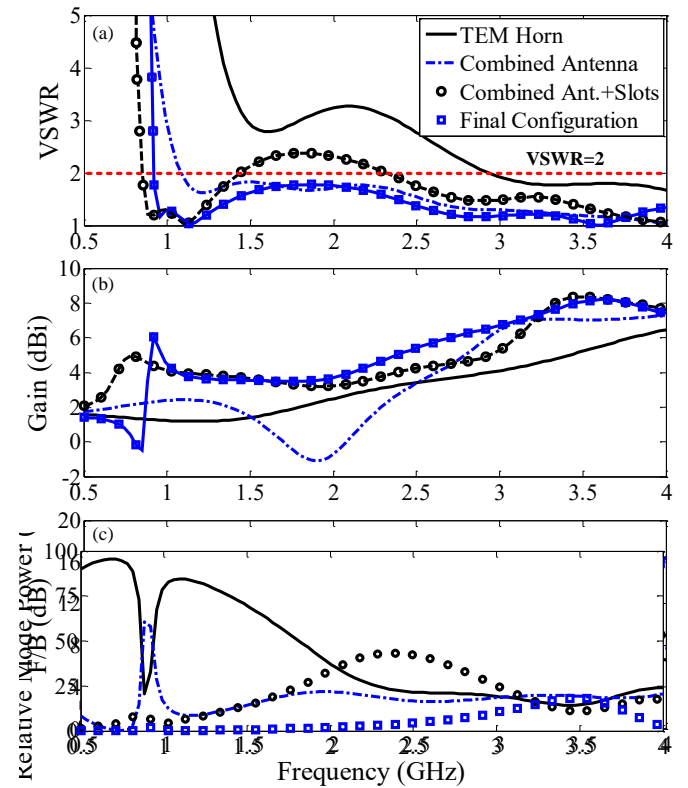


Fig.8. (a) VSWR, (b) gain, and (c) F/B of the studied configurations.

The improvements in impedance match, gain, and F/B due to the discussed phenomena are demonstrated in Fig. 8. The turn-on frequency is lowered to 0.84GHz as expected from the achieved balancing condition. VSWR slightly deteriorates between 1.4GHz and 2.4GHz . Gain of 4.72dBi is obtained at the turn-on frequency indicating ~ 3.5 and 2.5dB improvements compared to a conventional TEM horn and combined antenna; respectively. More consistent and higher gain is obtained over greater than $4:1$ bandwidth. F/B is also improved at low frequencies; however, one issue with this configuration is the drop in F/B over the mid band between 1.8GHz and 3GHz (see Fig. 8(c)). The chief reason for that is the reduced radiation of $TM_{\pm 11}$ modes over this frequency band as can be observed from Fig. 6(c). To enhance the radiation of $TM_{\pm 11}$ modes, bow-tie shaped plates (i.e. wideband electric dipole) are inserted at the position d_i measured from the loop's back plate as shown in Fig. 4(b). The location of the plates is chosen such that the currents

around 2GHz are redirected thereon resulting in the radiation of $TM_{\pm 11}$ modes over relatively wide band. The radiation improvement of these modes around 2GHz can be observed from the spherical mode spectrum in Fig. 5(d). More consistent $TM_{\pm 11}$ radiation is observed at the mid and high frequencies. Also, the inserted plates add another small loop to the geometry which tunes the radiation of fundamental $TE_{\pm 11}$ modes and consequently the modes-balancing frequency at the low end. The $TM_{\pm 12}$ modes radiation (mainly the phase response) is tuned as well due to the modifications of loop geometry. The obtained phase response of the fundamental and higher order modes approaches the desired criteria relatively better than the other configurations as shown in Fig. 6.

The performance of this configuration (referred as final configuration) is also shown in Fig. 8. As seen from Fig. 8(a), the turn-on frequency slightly increases to 0.9GHz as expected from the spherical mode spectrum in Fig. 5(d). The inserted plates tune the antenna's input impedance leading to a better impedance match over the band. As shown in Fig. 8(b), gain of 6dBi is obtained at the turn-on frequency and noticeably higher gain compared to the conventional configurations is obtained over the designated bandwidth of operation as expected from the demonstrated constructive modes combination. F/B is also improved with this topology as a result of enhanced radiation of $TM_{\pm 11}$ modes. As demonstrated in Fig. 8(c), $F/B > 9.5\text{dB}$ is achieved over the operating bandwidth. 3D-radiation patterns of the conventional TEM horn, combined antenna, and the proposed combined antenna (with the perturbation slots and plates) are shown at different frequencies in Figs. 9(a), (b), and (c); respectively. The bidirectional radiation characteristics of the conventional configurations are clearly demonstrated at low and mid bands. The final configuration shows noticeably enhanced directive radiation patterns with the desired cardioid shape at the low end, high F/B, and low back lobes over the band.

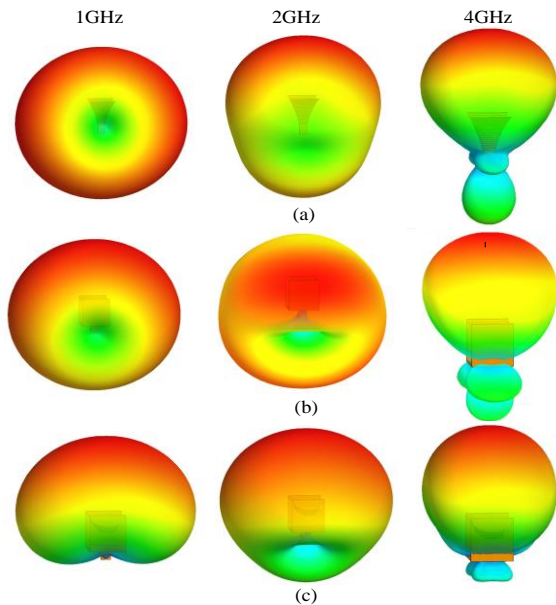


Fig.9. 3D-radiation patterns of (a) conventional TEM horn, (b) combined antenna, and (c) proposed combined antenna at different frequencies.

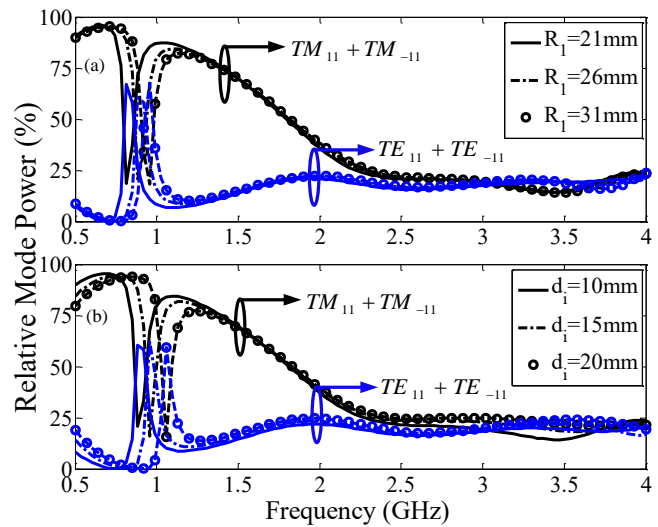


Fig.10. Effects of changing (a) R_1 and (b) d_i on the fundamental spherical modes of the proposed combined antenna.

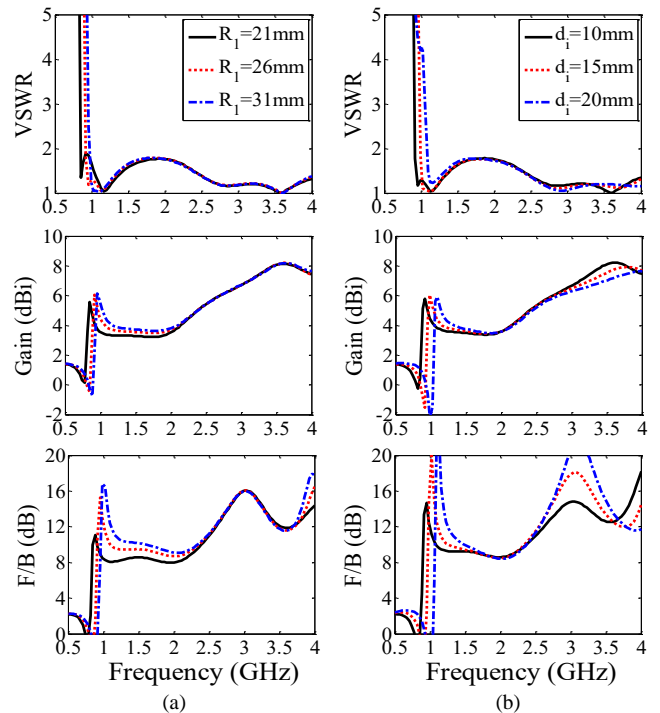


Fig.11. Effects of changing (a) R_1 and (b) d_i on the VSWR, gain, and F/B of the proposed combined antenna.

The proposed combined antenna has 3.3 times reduced turn-on frequency, noticeably higher gain and F/B, excellent impedance match, and superior radiation characteristics over more than two octaves bandwidth compared to the conventional TEM horn. At higher frequencies (above 4GHz), the TEM horn is dominant; thus, similar performance to that of a regular TEM horn is obtained. Note that the proposed antenna is not optimized at this point. The conducted parametric studies show that the magnitude and phase of the radiated modes can be controlled by modifying the antenna's geometrical parameters such the loop length (L_l), crescent slot parameters (R_1 or R_2) and the inserted plates location (d_i). For example, decreasing R_1 and d_i tunes the fundamental modes excitation and lower the turn-on frequency with slight

decrease in gain and F/B over the mid band as demonstrated in Figs. 10 and 11. d_i can also help controlling the gain and F/B at higher frequencies as shown in Fig. 11(b). The conducted numerical studies show that the combined antenna can be designed with electrical size (ka) of 0.79 at the turn-on frequency which is closely approaching the fundamental limit in [29]. From the spherical modes perspective, the proposed antenna gain can be improved even further by achieving a wideband excitation of the fundamental modes (at low frequencies) and fulfilling the desired phase criteria between the modes' coefficients which is currently being researched. The proposed combined antenna is also expected to have better time-domain performance. The features of low aperture reflection, high and consistent realized gain, high F/B, and definitely the low-dispersion characteristics of the TEM horn permit a high-quality pulse radiation operation.

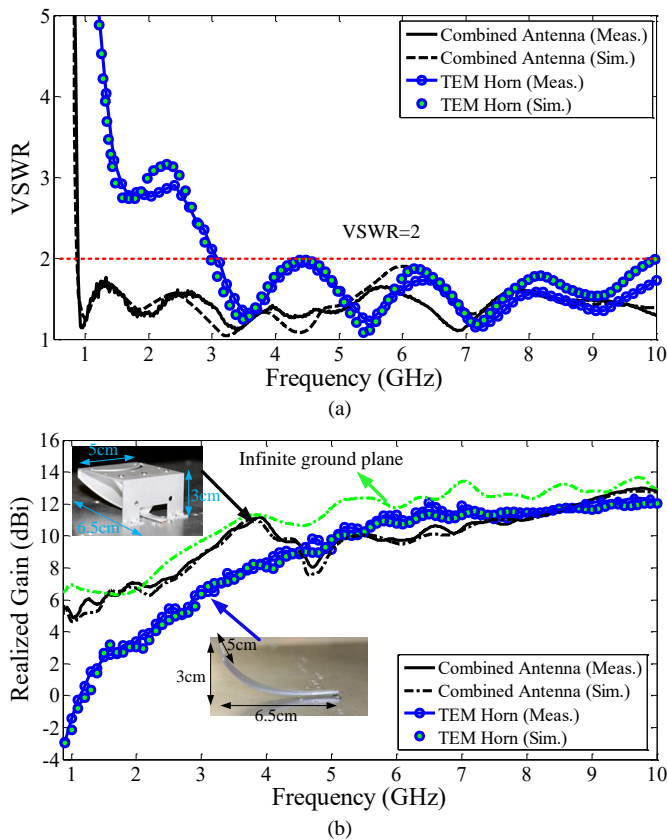


Fig.12. Measured and simulated (a) VSWR and (b) peak realized gain of the proposed combined antenna and conventional design shown in the inset.

IV. FREQUENCY- AND TIME-DOMAIN PERFORMANCES

To validate the above-discussed design concept, the proposed combined antenna is fabricated as a half-cut prototype placed over a ground plane. Realizing the antenna over ground plane simplifies the fabrication, eliminates the need for wideband balun, and enables a better match to 50Ω impedance. One issue is asymmetric E-plane radiation patterns which can be improved by increasing the size of the ground plane. The fabricated antenna is shown in Fig. 1 along with its geometrical details. As seen, the antenna is composed of three parts, specifically; TEM horn plate, loop built from rectangular plate with the crescent slot loading, and the bow-

tie plate placed between the horn and loop. These parts are built separately and assembled by metallic screws. The antenna is fed using SMA connector below the ($35\text{cm} \times 35\text{cm}$) ground plane. The separation between the TEM horn plate and the ground plane at the feed is 1mm.

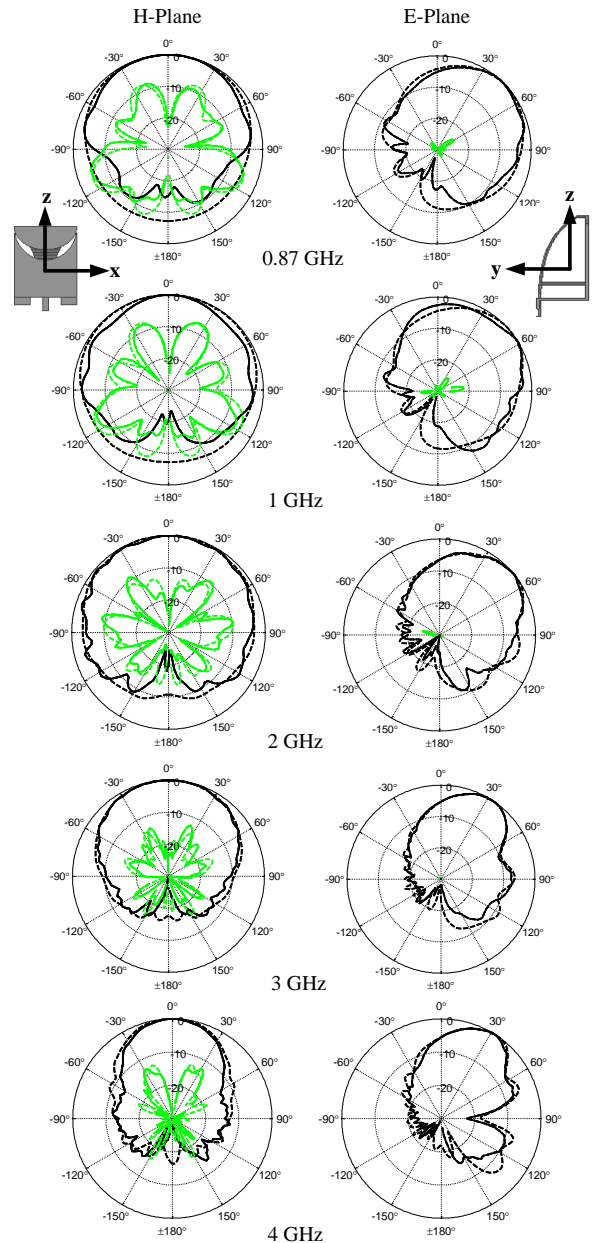


Fig.13. Measured (solid) and simulated (dashed) H- and E-plane co- (dark) and cross-polarized (light) radiation patterns of the combined antenna at different frequencies across the operating bandwidth.

A. Frequency-Domain Performance

The measured and simulated VSWRs of the proposed and conventional TEM horn antennas are shown in Fig. 12 (a). Significantly better impedance match is achieved with the combined antenna. The turn-on frequency is reduced more than 3 times (i.e. from 3GHz to 0.87GHz) while $\text{VSWR} < 1.7$ is measured over the desired bandwidth of operation. Notice that the conventional TEM horn and the proposed miniaturized horn have similar physical length, width, and height of 6.5cm,

5cm, and 3cm, respectively as shown in the inset of Fig. 12(b). Yet, the electrical sizes of the conventional and miniaturized designs are $0.65\lambda_{\text{turn-on}} \times 0.5\lambda_{\text{turn-on}} \times 0.3\lambda_{\text{turn-on}}$ and $0.188\lambda_{\text{turn-on}} \times 0.145\lambda_{\text{turn-on}} \times 0.087\lambda_{\text{turn-on}}$, respectively.

The measured and simulated peak realized gains are shown in Fig. 12(b) for both antennas. Up to 9dB higher gain is measured with the combined antenna at the low frequencies and noticeably higher gain is measured over the band. The simulated realized gain of the antenna over infinite ground plane is also plotted in Fig. 12(b) to demonstrate the effect of the finite-size ground plane on the antenna's gain. The antennas far-field measurements are conducted inside University of Colorado anechoic chamber. ETS-Lindgren 3115 standard gain horn is used to characterize antenna gain. The computed/measured antenna's radiation efficiency is $\sim 100\%$. As discussed, the combined antenna has similar performance to that of the conventional TEM horn at higher frequencies [30]. Consistent performance with high gain and $\text{VSWR} < 2$ are obtained over more than 10:1 bandwidth with the combined antenna. The demonstrated performance agrees with and validates the results from the previous Section.

The measured H- and E-plane co- and cross-polarized radiation patterns are shown in Fig. 13. Symmetric radiation patterns are obtained in H-plane. The E-plane patterns are squinted due to the finite-size ground plane. The takeoff angle decreases as the frequency increases. The cross-pol. is lower in E-plane and at horizon is below -30dB over the operating bandwidth. The increased cross-polarization in H-plane is due to the size and shape of the utilized ground plane [31]. Using a circular ground plane, increasing its size, or coating its edges with absorbing materials can help reducing the negative effects on radiation pattern.

B. Time-Domain Performance

The time-domain performance of the fabricated antenna is also characterized. The antenna transfer function is determined first using the two-antenna measurement technique [32]. With this apparatus, the transmission coefficient S_{21} between the antenna under test (AUT) and a reference antenna with known transfer function is measured in anechoic chamber at well-defined reference planes. Then, the radiation transfer function of AUT is obtained. Once the transfer function is measured, the radiated pulses are obtained by multiplying the input pulse spectrum by transfer function and transfer the result to time domain using the inverse Fourier transform (IFFT). In this work, S_{21} is measured inside the chamber using Agilent PNA-x 5245A. The reference antenna is kept fixed at the direction of maximum gain ($\theta = 0^\circ, \varphi = 0^\circ/90^\circ$) while the antenna under test (AUT) is rotated in elevation plane with $\Delta\theta = 3^\circ$ in E- and H-planes. Data are taken from 0.3 GHz to 8 GHz with 10 MHz resolution.

Measured and simulated group delay curves derived from the measured and simulated phase responses of the transfer function are shown in Fig. 14. Low group delay variation is obtained with the proposed antenna indicating low dispersion characteristics. These group delay curves suggest that the antenna can radiate short pulses (with pulse width $< 1\text{ns}$) without any significant distortion.

To assess the amount of distortion incurred to a wideband signal by this antenna, a second-derivative Gaussian pulse is used as input pulse. The utilized pulse, shown in the inset of Fig. 14, is defined as,

$$v_t(t) = \left(\frac{1}{\sqrt{2\pi}\sigma^3} - \frac{(t-t_o)^2}{\sqrt{2\pi}\sigma^5} \right) \exp\left(-\frac{(t-t_o)^2}{2\sigma^2} \right) \quad (9)$$

where t_o is the time shift (chosen to be 0.5 ns), and σ is the parameter that controls the pulse width. For herein study, σ value of 80ps is used to achieve power spectral density with 5:1 10dB-bandwidth from 1GHz to 5GHz.

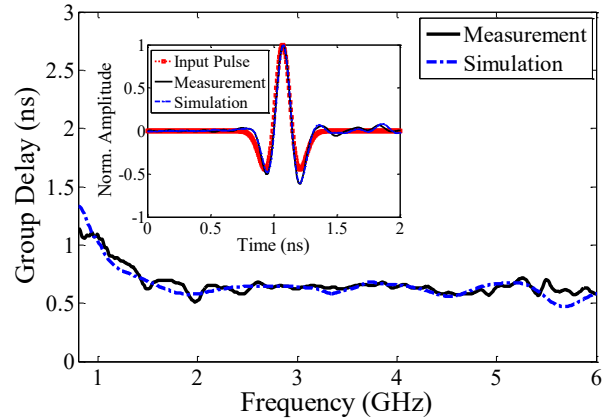


Fig.14. Measured and simulated group delay of the combined antenna. Input, measured, and simulated radiated pulses are also shown in the inset.

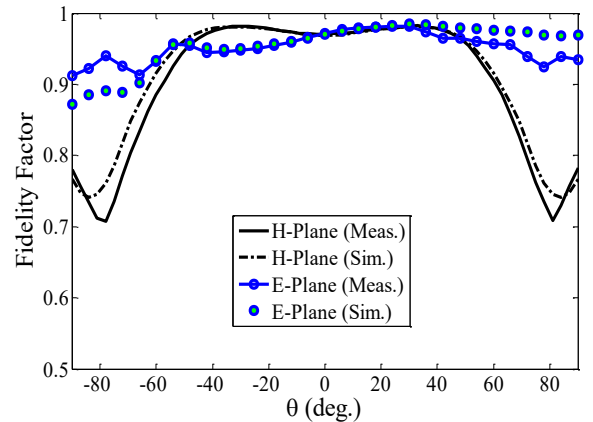


Fig.15. Measured and simulated E- and H-plane fidelity factor.

The corresponding measured and simulated (obtained from CST MWS transient solver) radiated pulses along the antenna axis are also shown in Fig. 14. As seen; pulses with a shape almost identical to the input pulse shape and low ringing are radiated. The fidelity factor is used [32] to characterize the quality of the radiated pulses over the field of view. As seen from Fig. 15, fidelity factor above 0.95 is obtained over wide field of view in E- and H-plane indicating high-quality time-domain performance. Notice that fidelity factor of 1 means that the input and radiated pulses are identical. Excellent agreement between measurement and simulation throughout this section in both domains is a testament to the soundness of the proposed design approach.

V. CONCLUSION

The design and miniaturization of a combined TEM horn-loop antenna is discussed. The spherical mode expansion technique is used to investigate the characteristics of the excited modes and simple geometrical modifications are implemented to achieve desired modes' combination. Engineering of spherical modes may enable a systematic and simplified design and significant reduction in the number of required parametric studies. The fabricated combined antenna has a significantly reduced volume, low-profile, improved gain and F/B, and better radiation characteristics compared to a conventional design. Excellent time-domain performance quantified by high fidelity factor is also obtained. The demonstrated features make the proposed combined antenna a visible candidate for different time- and frequency-domain applications.

REFERENCES

[1] J. D. Taylor, "Ultra-wideband radar overview," in *Introduction to Ultra-Wideband Radar Systems*. Boca Raton, FL: CRC Press, 1995, ch. 1.

[2] B. Allen, M. Dohler, E. Okon, W. Malik, A. Brown, and D. Edwards, *Ultra Wideband Antennas and Propagation for Communications, Radar and Imaging*. West Sussex, UK: Wiley, 2006.

[3] R. T. Lee and G. S. Smith, "A design study for basic TEM horn antenna," *IEEE Antennas Propag. Mag.*, vol. 46, no. 1, pp. 86–92, Feb. 2004.

[4] A. E-C. Tan, K. Jhamb, and K. Rambabu, "Design of transverse electromagnetic horn for concrete penetrating ultrawideband radar," *IEEE Trans. Antennas Propag.*, vol.60, pp. 1736-1743, Apr. 2012.

[5] S. Evans and F. N. Kong, "TEM horn antenna: Input reflection characteristics in transmission," *IEE Proc.*, vol. 130, no. 6, pt. H, pp. 403–409, Oct. 1983.

[6] K. Chung, S. Pyun, and J. Choi, "Design of an ultrawide-band TEM horn antenna with a microstrip-type balun," *IEEE Trans. Antennas Propag.*, vol. 53, no. 10, Oct. 2005.

[7] R. J. Wohlers, *The GWIA, an extremely wide bandwidth low-dispersion antenna*. Buffalo, New York: Calspan Corporation, 1971.

[8] Y. Chen, Y. Wang, Q. Wang, "A new type of TEM horn antenna for high-altitude electromagnetic pulse simulator," *IEEE Antennas Wireless Propag. Lett.*, vol. 12, p. 1021–1024, 2013.

[9] M. Kanda, "The effects of resistive loading of "TEM" horns," *IEEE Trans. Electromagn. Compat.*, vol. EMC-24, no. 2, pp. 245–255, May 1982.

[10] M. Elmansouri and D. Filipovic, "Reduced-size TEM horn for short-pulse high-power electromagnetic systems," in *Proc. IEEE Antennas Propag. Soc. Int. Symp. (APSURSI)*, Memphis, TN, Jul. 2014, pp.828–829.

[11] A. S. Turk and D. A. Sahinkaya, "Partial dielectric loaded TEM horn design for ultra-wideband ground penetrating impulse radar systems," in *Ultra-Wideband, Short-Pulse Electromagnetics 7*, pp. 306–315, Springer, Berlin, Germany, 2007, ch. 34.

[12] C.E. Baum, "Low-frequency compensated TEM horn," *Sensor and Simulation Notes*, Jan. 1995, Note 377.

[13] M. H. Vogel, "Design of the Low-Frequency Compensation of an Extreme-Bandwidth TEM Horn and Lens IRA," in *Ultra-Wideband Short-Pulse Electromagnetics 3*, pp. 97-105, New York, NY, Plenum Press, 1997.

[14] A. Elsherbini and K. Sarabandi, "ENVELOP antenna: a class of very low profile UWB directive antennas for radar and communication diversity applications," *IEEE Trans. Antennas Propag.*, vol.61, no.3, pp.1055–1062, Mar. 2013.

[15] X. Liu, G. Wang, and W. Wang, "Design and performance of TEM horn antenna with low-frequency compensation," in *Proc. Asia-Pacific Conf. Environ. Electromagn. (CEEM2003)*, Hangzhou, China, Nov. 2003, pp. 306-309.

[16] H. Park, J. Kim, J. Ryu, J. Choi, and Y. Yoon, "Modified low-frequency compensated TEM (LFCTEM) horn antenna to improve the

radiation performance," in *Proc. Asia-Pacific Microw. Conf. (APMC)*, Seoul, South Korea, Nov. 2013, pp. 1163-1165.

[17] Y. A. Andreev, Y. I. Buyanov, and V. Koshelev, "Combined antennas for high-power ultra wideband pulse radiation," in *Proc. 14th Int. Symp. on High Current Electronics*, Tomsk, Russian Federation, Sep. 2006, pp. 435–438.

[18] A. R. Mallahzadeh and F. Karshenas, "Modified TEM horn antenna for broadband applications," *Prog. Electromagn. Res.*, vol. 90, pp. 105–119, 2009.

[19] J. E. Hansen *et al.*, *Spherical Near-Field Antenna Measurements*, ser. IEE Electromagnetic Waves Series. London, U.K.: Peter Peregrinus, 1988, vol. 26.

[20] FEKO EM Software and Systems, Pty Ltd., Stellenbosch, South Africa.

[21] B. Brock "Using vector spherical harmonics to compute antenna mutual impedance from measured or computed fields," Sandia National Laboratories, Albuquerque, NM, 2001, Sandia Rep. SAND2000-2217-Revised.

[22] P. L. Overfelt, D. R. Bowling, and D. J. White, "A collocated magnetic loop, electric dipole array antenna (preliminary results)," *NAWCWPNS Tech. Pub.* 8212, China Lake, CA, Sept. 1994.

[23] J. S. McLean and R. Sutton, "Practical realization of PxM antennas for high-power, broadband applications," *Ultra-Wideband, Short-Pulse Electromagnetics 7*, pp. 267–275, Springer, Berlin, Germany, 2007, ch. 30.

[24] T. Belmaddem, L. Rudant, and T. P. Vuong, "Small antenna radiation properties analysis using spherical wave expansion," *15th Int. Symp. Antenna Tech. Appli. Electrom. (ANTEM)*, Toulouse, France, Jun. 2012, pp.1–5.

[25] R. F. Harrington, *Time-Harmonic Electromagnetic Fields*. New York, NY, USA: McGraw-Hill, 1961.

[26] D.-H. Kwon, "Radiation Q and the gain of TM and TE sources in phase delayed rotated configurations," *IEEE Trans. Antennas Propag.*, vol. 56, no. 8, pp. 2783–2786, Aug. 2008.

[27] M. Elmansouri and D. S. Filipovic, "Design of combined-antennas using spherical modes," in *Proc. Antenna App. Symp.*, Monticello, IL, Sept. 2014, pp.167–187.

[28] C. E. Baum, "Combined electric and magnetic dipoles for mesoband radiation," *Sensor and Simulation*, Aug. 2007, Note 523.

[29] B. A. Kramer, C.-C. Chen, M. Lee, and J. L. Volakis, "Fundamental limits and design guidelines for miniaturizing ultra-wideband antennas," *IEEE Antennas Propag. Mag.*, vol. 51, no. 4, pp. 57–69, Aug. 2009.

[30] M. Elmansouri, and D. S. Filipovic, "Miniaturization of TEM Horn Antenna Using Spherical Modes," 2014 *AMEREM*, Albuquerque, NM, Jul. 2014.

[31] H. Arai, *Measurement of Mobile Antenna Systems*. Boston, MA: Artech House, 2001, ch. 2.

[32] C. Roblin, "Representation, Characterization, and Modeling of Ultra Wide Band Antennas," in *Ultra Wide Band Antennas*, ch. 3, NJ: John Wiley, 2011.



Mohamed A. Elmansouri (S'10-M'2013) received his B.S. and M.S. degrees in electrical engineering from University of Tripoli, Libya, in 2005 and 2008, respectively, and Ph.D. degree from University of Colorado, Boulder, in 2013. He is currently a Senior Research Associate at the University of Colorado Boulder, where his interests are in broadband antennas, frequency-independent antennas, high-power arrays, STAR systems, and computational and applied electromagnetics.



Dejan S. Filipovic (S'97-M'02-SM'08) received the Dipl. Eng. degree from the University of Niš, Serbia, in 1994, and Ph.D. degree from The University of Michigan at Ann Arbor in 2002. Currently, he is a Charles Victor Schelke Endowed Professor at the University of Colorado Boulder. His research interests are antenna theory and design, modeling and design of passive millimeter-wave components and systems, as well as computational and applied electromagnetics. Mr. Filipovic was the recipient of the Nikola Tesla Award, Holland's Teaching Award, two Provost's Faculty Achievement Awards, and several best conference paper awards.